Available online at www.sciencedirect.com

SciVerse ScienceDirect

Ceramics International 39 (2013) 7831–7838

CERAMICS INTERNATIONAL

www.elsevier.com/locate/ceramint

Improved pseudo-capacitive performance of manganese oxide films synthesized by the facile sol–gel method with iron acetate addition

Chien Chon Chen[a], Chia-Yu Yang[b], Chung-Kwei Lin[c,*]

[a]Department of Energy Engineering, National United University, Miaoli 36003, Taiwan
[b]Department of Materials Science and Engineering, Feng Chia University, Taichung 40724, Taiwan
[c]School of Dental Technology, College of Oral Medicine, Taipei Medical University, Taipei 11031, Taiwan

Received 7 February 2013; received in revised form 11 March 2013; accepted 13 March 2013
Available online 25 March 2013

Abstract

Manganese oxide electrodes possessing pseudo-capacitance behaviors were successfully made with a simple sol–gel method. The experimental results showed that the specific capacitance was 101.2 F/g for pure manganese oxide films after annealing at 300 °C. However, the specific capacitance increased to 232.3 F/g with iron acetate (1.0 mol% Fe) addition and after annealing at 350 °C. The surface morphology observations revealed that the annealing temperature of 350 °C produced a higher surface area film with smaller pores. X-ray diffraction results showed that the manganese-iron oxide was composed of Mn_3O_4 and Mn_2O_3 phases, without iron oxide diffraction peaks. The manganese-iron oxide electrode with Mn_3O_4 and Mn_2O_3 phases exhibited good electrochemical performance and capacitance efficiency.

Keywords: Pseudo-capacitance; Sol–gel; Specific capacitance; Manganese acetate; Iron acetate

1. Introduction

Electrochemical capacitors (ECs) are expected to have a high degree of reversibility and a much longer cycle (10^4–10^6 cycles with RuO_2). ECs store the electric energy in an electrochemical double layer [1]. The electrochemical capacitors are also called double layer capacitors, super-capacitors, ultra-capacitors, or pseudo-capacitors. The double layer capacitance is about 10–20 mF/cm^2 for a smooth electrode in concentrated electrolyte solution, with a high electric field value assumed up to 10^6 V/cm [2]. The capacitance can be estimated by assuming a high surface area of carbon with 1000 m^2/g and a double layer capacitance of 10 mF/cm^2 [3]. The theoretical maximum achievable energy densities of an EC can be expressed as 100 F/cm^3 [4]. The pseudo-capacitance arises from fast, reversible, and Faradaic redox reactions that occur within the bulk material of the electrode over an appropriate range of potentials [5]. In the case of pseudo-capacitors, the Faradaic charge transfer occurs between electrolyte and electrode. Various noble and transition metal oxides, such as RuO_2, IrO_2, NiO_2, CoO_x, SnO_2, and MnO_2, have been used as electrode materials [6–10]. The oxide of RuO_2 has the highest pseudo-capacitance, greater than 650 F/g [11]. However, the expense of materials and the pollution of electrolytes restrict the application of RuO_2. On the other hand, the surface area and pore distribution of the comparatively inexpensive MnO_2 can be controlled by simply adjusting the reaction time and the content of surfactant in the aqueous phase. Therefore, MnO_2 is widely applied as a battery and capacitor material. The theoretical specific capacitance of MnO_2 can be 1370 F/g [11,12]; however, the practical specific capacitance is low due to the intrinsically poor electronic conductivity and dense morphology of the oxide. Two efficient ways to raise the specific capacitance of MnO_2 are to increase the surface area with nanostructured MnO_2 [13] and to increase electronic conductivity with added carbon nanotubes in the MnO_2 matrix [14]. The high power property of the electro-active species is one of the basic requirements for the electrode materials of electrochemical super-capacitors. This electrochemical property is strongly dependent on the electrochemical kinetics of redox transitions. The specific capacitance, C (F/g), of given composite electrodes can be determined by integrating the cyclic voltammogram (CV) curve with an applied polarization voltage

*Corresponding author. Tel.: +8862 2736 1661x5115.
E-mail address: chungkwei@tmu.edu.tw (C.-K. Lin).

0272-8842/$ - see front matter © 2013 Elsevier Ltd and Techna Group S.r.l. All rights reserved.
http://dx.doi.org/10.1016/j.ceramint.2013.03.043

(ΔE) to obtain the voltammetric charge (Q), and subsequently dividing this charge by the mass of the composite electrode (m) to get the specific capacitance: $C = Q/(\Delta E m)$ [15].

Surface area and crystallization directly affect the electrochemical kinetics of redox transitions. In this study, we present a simple and inexpensive process for directly forming pseudo-capacitor manganese oxide electrodes with iron acetate addition with a sol–gel method. In this study, we also focus on the electrode morphology measurement with the quantity of the addition of Fe and the annealing temperature of the electrode. Due to the addition of iron acetate, the surface and electronic conductivity of pseudo-capacitors increased. The corresponding material, microstructure, phase transformation, and electrochemical characteristics were examined systematically. The Fe/Mn content ratio within the oxide was controlled by adjusting the iron acetate concentration in the manganese acetate deposition solution. The deposited oxides were characterized by differential scanning calorimetry (DSC), thermal gravimetric analysis (TGA), scanning electron microscopy (SEM), transmission electron microscopy (TEM), X-ray diffraction (XRD), extended X-ray absorption fine structure (EXAFS), radial distribution functions (RDF) spectra, and cyclic voltammetry (CV).

2. Experimental procedures

Manganese oxide films without or with ironic acetate ($C_4H_7FeO_5$) addition (0.5, 1.0, 2.0, 2.5, 5.0, and 7.5 mol% Fe) were prepared on graphite substrates by sol–gel and drop coating methods. The mol% Fe of the ratio of manganous acetate Mn $(CH_3COO)_2$ and iron acetate are shown in Table 1. The pseudo-capacitive electrodes were fabricated on graphite substrates as follows: (1) graphite substrate ($1 \times 1 \times 0.5$ cm^3) was cleaned in 0.2 M sulfuric acid (H_2SO_4) solution, and flushed by de-ionized water; (2) 10.509 g citric acid ($C_6H_8O_7$) was added to 149.29 ml propanol alcohol ($CH_3CH_2CH_2OH$) under supersonic wave shaking for 1 h and stirring for 12 h to make a solvent; (3) to the solvent was added 6.127 g manganous acetate; (4) ammonium hydroxide (NH_4OH) was dipped into the solution from step (4) to adjust the pH value (9.6) of the solution; (5) ironic acetate was added into the solution from step (4) and stirred for 12 h, making 0.5, 1.0, 2.0, 2.5, 5.0, and 7.5 mol% Fe/Mn sol; (6) when the sol was obtained, it was slowly dipped on the graphite substrates, dried at room temperature for 15 min, heated at 80 °C for 1 h, and then annealed in an air oven at 250, 300, 350, and 400 °C for 1 h, respectively. The amount of deposited manganese oxide was measured by weighing the electrode with a microbalance (ME235S, Sartorius).

The endothermic/exothermic reactions of the manganese iron oxide films were detected from 50 to 600 °C by differential scanning calorimetry (DSC, MDSC29, TA Instrument) and thermal gravimetric analysis (TGA 2950, TA Instrument). The phases of the manganese iron oxide films were identified by X-ray diffractometry (XRD, MAC-MXP3, Japan) with Cu Kα radiation. Electrochemical measurements of cyclic voltammetry (CV) performances were evaluated by an electrochemical analyzer (CH Instruments, Model 600B, USA) using a standard three-electrode cell system with platinum and saturated calomel electrode (SCE) as the counter and reference electrodes in 1 M Na_2SO_4 (pH ~ 6.0) solution at room temperature. In the CV experiments, the potential scan rate was set at 25 mV/s within a

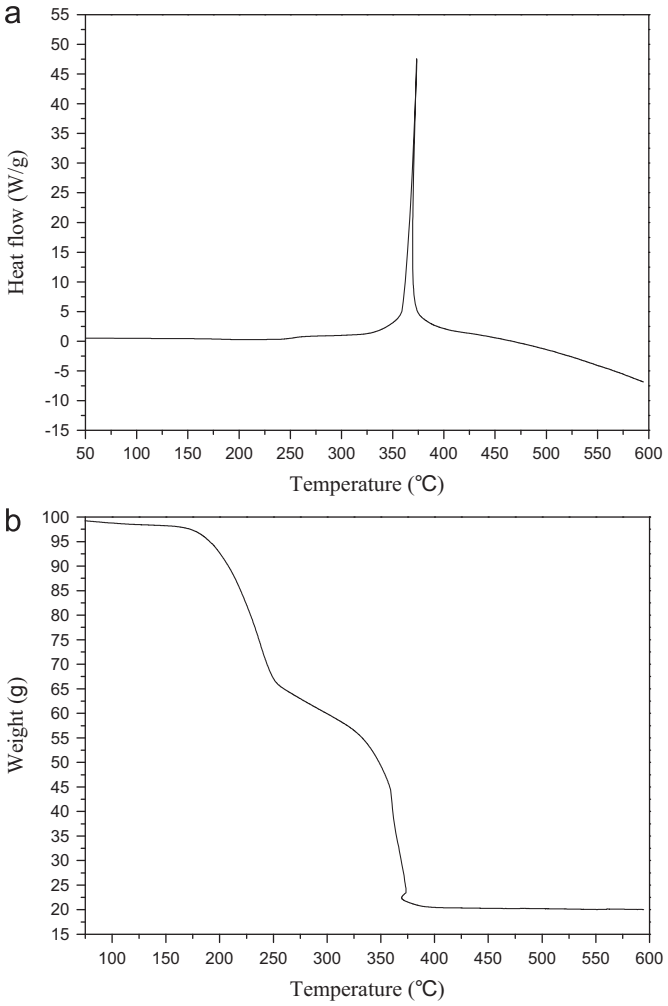

Fig. 1. The thermal characteristics of manganese oxide gel between 25 and 600 °C: (a) DSC curve of a heat flow peak present between 350 and 370 °C with Mn_2O_3 phase transfer to Mn_3O_4 phase. (b) TGA curve of five obvious weight loss regions: water molecule evaporation region (25–170 °C), organic matter removal region (170–250 °C), $Mn(OH)_x$ decomposition to the Mn_3O_4 and Mn_2O_3 regions (250–350 °C), Mn_3O_4 phase change to Mn_2O_3 region (350–400 °C), and stable Mn_2O_3 phase region (400–600 °C).

Table 1
Summary of mol% Fe by various of ratio of manganese acetate and iron acetate.

mol% Fe	0 mol% Fe	0.5 mol% Fe	1.0 mol% Fe	2.0 mol% Fe	2.5 mol% Fe	5.0 mol% Fe	7.5 mol% Fe
$Mn(CH_3COO)_2$ (g)	6.127	6.097	6.066	6.005	5.974	5.821	5.668
$C_4H_7FeO_5$ (g)	0	0.024	0.048	0.095	0.119	0.239	0.358

potential range of 0–1 V (SCE). The micro-morphologies of the heat-treated electrodes before and after CV tests were examined using a scanning electron microscope (FE-SEM, HITACHI S4800, Japan). X-ray absorption spectroscopy measurements were performed at the Wiggler C (4–15 keV) and HSGM (110–1500 eV) beam lines of the National Synchrotron Radiation Research Center (NSRRC) in Hsinchu, Taiwan.

3. Results and discussion

In order to understand the basic characteristics and details of the heat treatment conditions, DSC and TGA tests were used for the manganese oxide gel. Fig. 1 shows the thermal characteristics of manganese oxide gel between 25 and 600 °C with a temperature increase rate of 5 °C/min: (a) DSC curve of a heat flow peak present between 350 and 370 °C with Mn_2O_3 phase transfer to Mn_3O_4 phase. (b) TGA curve showing five obvious weight loss regions: water molecule evaporation region (25–170 °C), organic matter removal region (170–250 °C), $Mn(OH)_x$ decomposition to the Mn_3O_4 and Mn_2O_3 regions (250–350 °C), CH_3COOH decomposition and Mn_3O_4 phase change to the Mn_2O_3 region (350–400 °C), and stable Mn_2O_3 phase region (400–600 °C). Because water molecules and organics evaporate below 250 °C and the stable Mn_2O_3 phase forms above 600 °C, annealing temperatures of 250, 300, 350, and 400 °C were chosen for our experiments. Fig. 2 shows XRD patterns with (a) pure manganese oxide powders composed of Mn_3O_4 and Mn_2O_3 phases after annealing at 250 °C; the intensity of Mn_2O_3 increased, but Mn_3O_4 decreased as temperature increased, which means Mn_3O_4 phase transformed into Mn_2O_3. (b) Manganese oxide gel with 1.0 mol% Fe addition, amorphous at 250 °C, Mn_2O_3 and Mn_3O_4 phases after annealing at 300 °C.

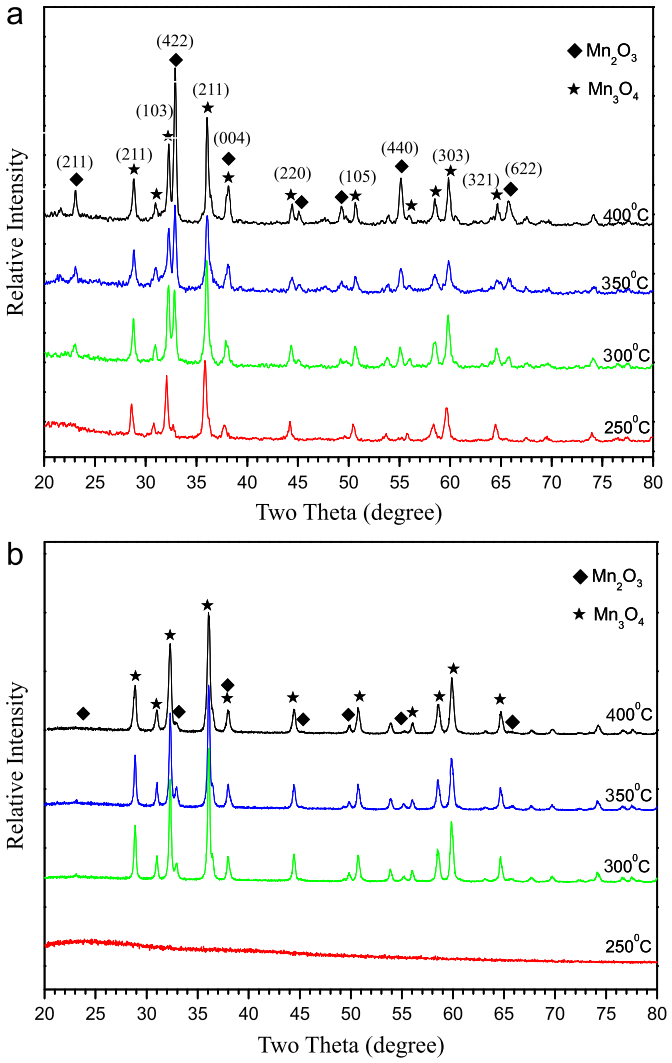

Fig. 2. XRD patterns with (a) pure manganese oxide gel with Mn_3O_4 and Mn_2O_3 phases; after annealing at 250 °C, the intensity of Mn_2O_3 increased, but Mn_3O_4 decreased as temperature increased, indicating that Mn_3O_4 phase transformed into Mn_2O_3. (b) Manganese oxide gel with 1.0 mol% Fe addition; amorphous after annealing at 250 °C, Mn_2O_3 and Mn_3O_4 phases after annealing at 300 °C. The intensity 0f Mn_3O_4 increased, but Mn_2O_3 decreased as temperature increased, indicating that Mn_2O_3 phase transformed into Mn_3O_4.

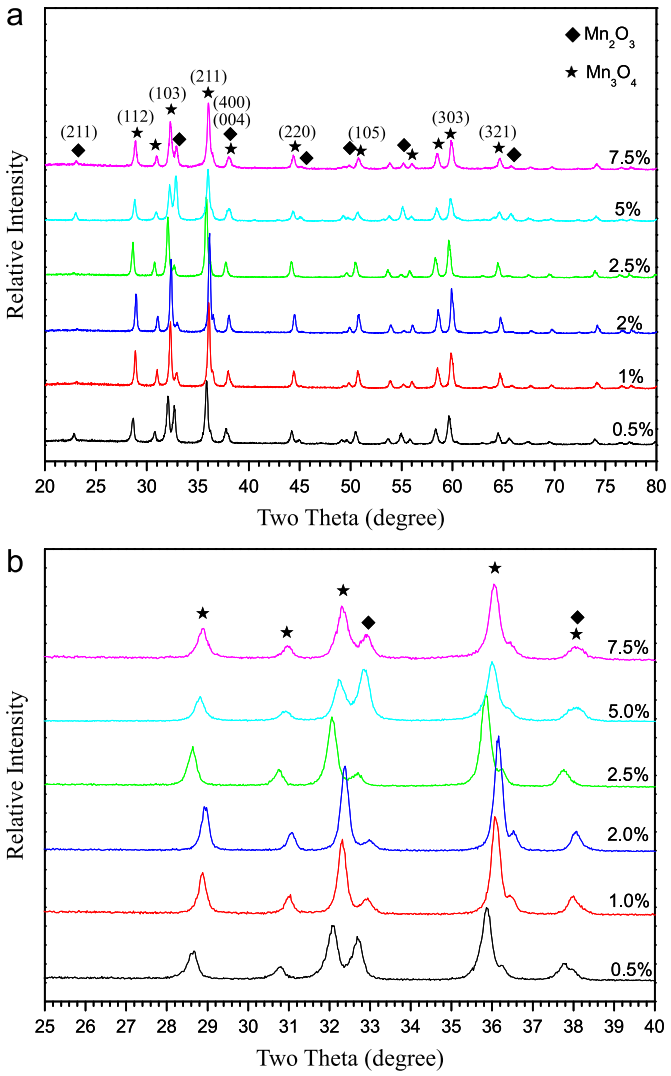

Fig. 3. XRD patterns of manganese oxide: (a) Peaks shift with Fe addition of 0.5, 1.0, 2.0, 2.5, 5, and 7.5 mol% compared to pure manganese oxide after annealing at 350 °C. (b) Peaks shifted to higher 2θ value when 0–2.0 mol% Fe was added to manganese oxide (Fe dissolves in the manganese oxide), and peaks shifted back to lower 2θ value when 2.0–2.5 mol% Fe was added to manganese oxide (precipitated).

The intensity of Mn_3O_4 increased, but Mn_2O_3 decreased as temperature increased, indicating that Mn_2O_3 phase transformed into Mn_3O_4. Fig. 3 shows XRD patterns of manganese oxide with various amounts of Fe added: (a) Because the lattice of manganese oxide was deformed by Fe addition, the XRD peaks shifted with Fe addition of 0.5, 1.0, 2.0, 2.5, 5, and 7.5 mol% as compared to pure manganese oxide after annealing at 350 °C. (b) Peaks shifted to a higher 2θ value when 0–2.0 mol% Fe was added to manganese oxide (Fe dissolves in the manganese oxide), and peaks shifted back to a lower 2θ value when 2.0–2.5 mol% Fe was added to manganese oxide (precipitated).

Fig. 4 shows SEM images of (a) rough and porous graphite substrate surface, which offers a large surface area, good adhesion for manganese oxide, and good conductivity for pseudo-capacitor; (b) manganese oxide with 1.0 mol% Fe addition; a thick amorphous layer covered the surface of the graphic substrate, and the surface was smooth after annealing at 250 °C because of retained amorphous organic matter and

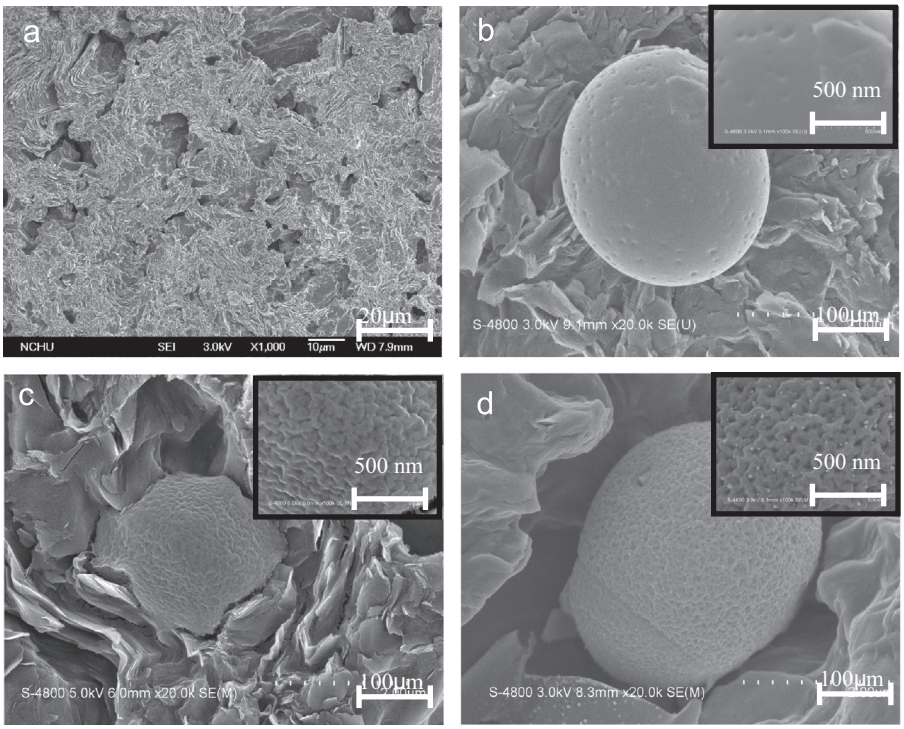

Fig. 4. SEM image of (a) graphite substrate surface, and (b) manganese oxide with 1.0 mol% Fe addition; an amorphous, smooth surface after annealing at 250 °C, (c) Mn_2O_3 and Mn_3O_4 phases, rough and corrugated surface after annealing at 300 °C, (d) Mn_2O_3 phases, rough, corrugated, and pitted surface after annealing at 350 °C.

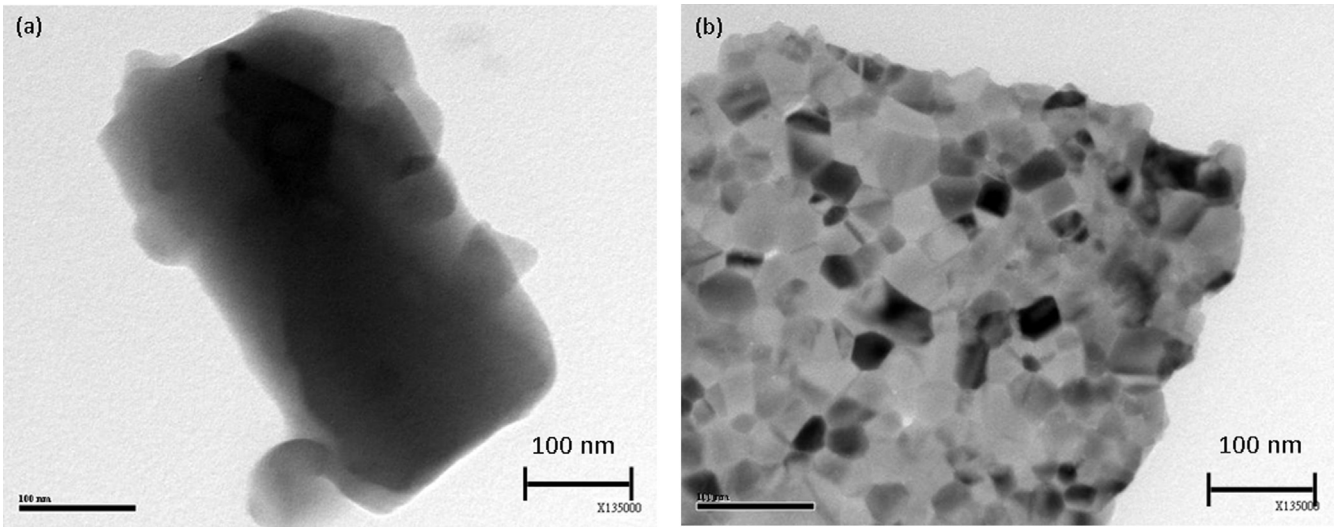

Fig. 5. TEM image of manganese oxide with 1.0 mol% Fe addition: (a) amorphous phase formed after annealing at 250 °C and (b) Mn_2O_3 phase after annealing at 350 °C.

$Mn(OH)_x$; (c) after the surface amorphous layer was removed, the Mn_2O_3 and Mn_3O_4 phases of the rough and corrugated surface presented after annealing at 300 °C. Because of the removal of organic matter, the porous particles formed in the laminated shape area; and (d) Mn_2O_3 phases of rough, corrugated, porous, and pitted surface after annealing at 350 °C. From the above results, we can conclude that the laminated shape area, porous, and pitted surface formations increased the contact area of electrolyte and electrode. Fig. 5 shows TEM images of manganese oxide with 1.0 mol% Fe

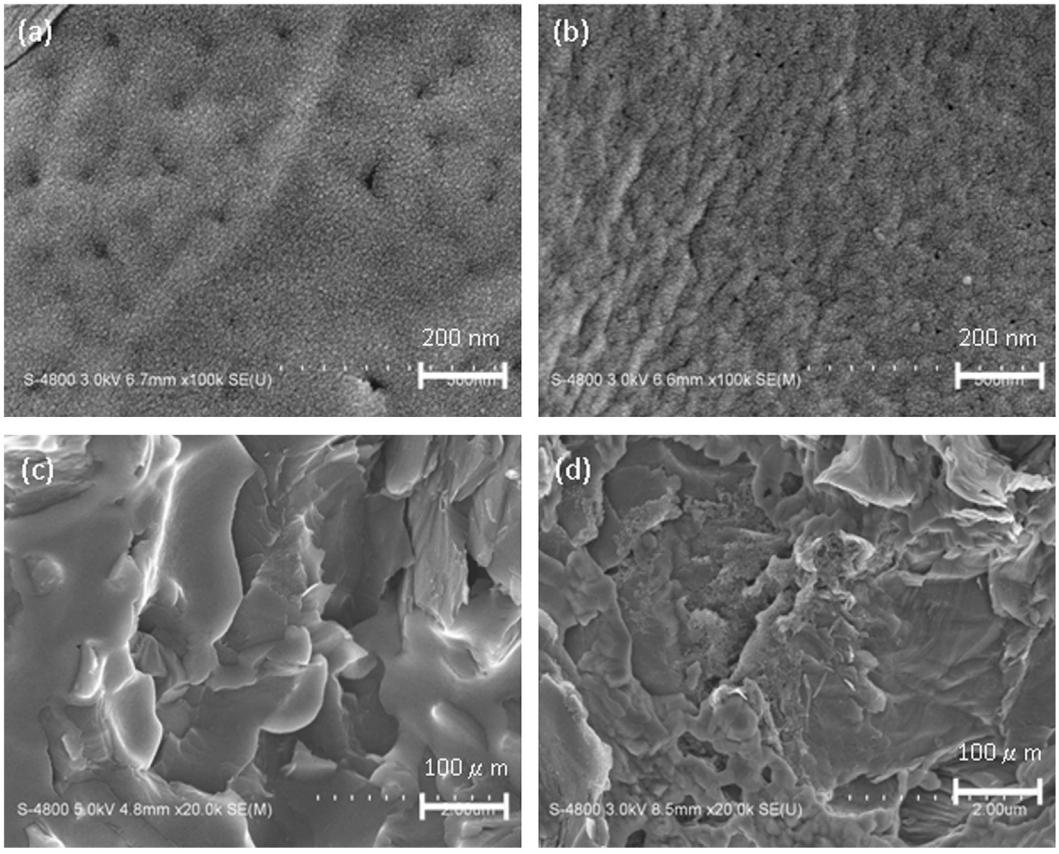

Fig. 6. SEM image of pseudo-capacitance electrode of manganese oxide with 1.0 mol% Fe addition on graphite substrate: (a) big hole formation when organic matter was removed after annealing at 250 °C, (b) Mn_2O_3 phases of rough, corrugated, and pitted surface after annealing at 350 °C, (c) collapsed film structure after annealing at 250 °C and CV testing, and (d) sheet film with holes structure after annealing at 350 °C and CV testing.

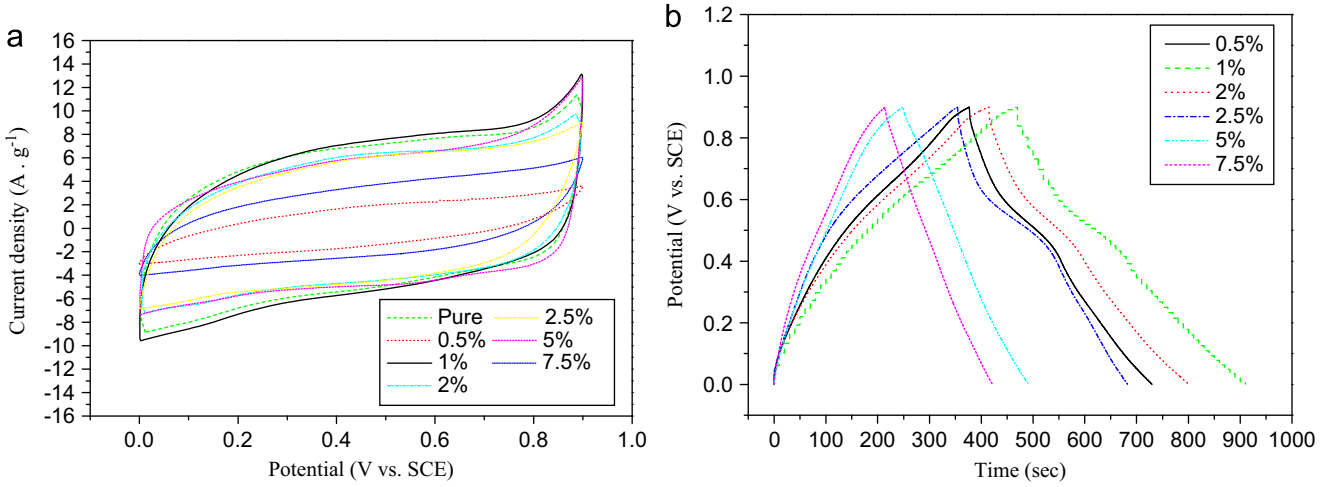

Fig. 7. Performance test curves of pseudocapacitive manganese oxide films with 0, 0.5, 1.0, 2.0, 2.5, 5.0 and 7.5 mol% Fe addition after annealing at 250, 300, 350, and 400 °C. Manganese oxide films with 1.0 mol% Fe addition annealed at 350 °C had the highest specific capacitance value, 232.3 F/g, on the (a) CV curves and (b) charge–discharge curve.

addition: (a) amorphous phase with organic matter retained after annealing at 250 °C and (b) 30–80 nm crystal size of Mn_2O_3 phase formation after annealing at 350 °C.

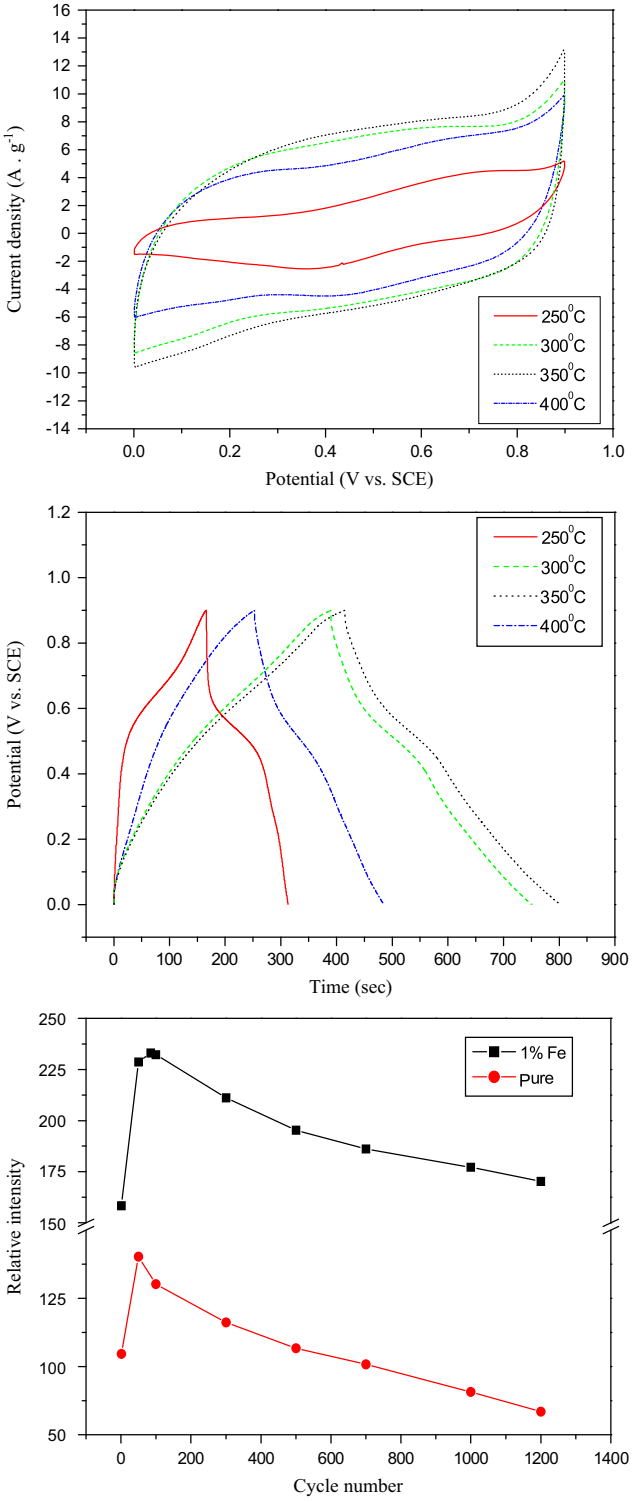

Fig. 8. Performance test curves of pseudocapacitive manganese oxide films with 1.0 mol% Fe addition after annealing at 250, 300, 350, and 400 °C annealing. Manganese oxide films with 1.0 mol% Fe addition annealed at 350 °C had the highest specific capacitance value after the 1200th cycle CV test: (a) curve, (b) charge–discharge curve, and (c) specific capacitance curve.

Fig. 6 shows SEM images of the pseudo-capacitance electrode of manganese oxide with 1.0 mol% Fe addition on graphite substrate: (a) Bigger hole formation after organic matter removal after annealing at 250 °C, (b) Mn_2O_3 phases of rough, corrugated, and surface after annealing at 350 °C, (c) collapsed structure of film after annealing at 250 °C and CV testing, and (d) sheet film with holes structure after annealing at 350 °C and CV testing. The SEM results shows that the electrode, after annealing at 350 °C, had a large surface area, with rough, corrugated, and pitted morphology.

Fig. 7 shows the performance test curves of pseudo-capacitive manganese oxide films with 0, 0.5, 1.0, 2.0, 2.5, 5.0 and 7.5 mol% Fe addition after annealing at 250, 300, 350, and 400 °C. Manganese oxide films with 1.0 mol% Fe addition after annealing at 350 °C had the highest specific capacitance value, 232.3 F/g, on the (a) CV curves and (b) charge–discharge curve. Furthermore, Fig. 8 shows the performance test curves of pseudo-capacitive manganese oxide films with 1.0 mol% Fe addition after annealing at 250, 300, 350, and 400 °C. Manganese oxide films with 1.0 mol% Fe addition after annealing at 350 °C had the highest specific capacitance value after the 1200th cycle CV test in the (a) CV curve and (b) charge–discharge curve, and (c) the pure manganese oxide and manganese oxide films with 1 mol% Fe addition had specific capacitance values of 36.3 F/g (49.3% decrease compared to the 1st cycle CV test) and 180.3 F/g (22.4% decrease compared to the 1st cycle CV test), respectively. The decrease in capacitance after cycling can also be attributed to increased electrode resistance with increasing cycle number. The specific capacitance (F/g) of manganese oxide electrode with various Fe additions and annealing temperature are summarized in Table 2.

Fig. 9 shows the characteristics of manganese oxide film with 1.0 mol% Fe addition after annealing at 250, 300, 350, and 400 °C: (a) Synchrotron X-ray absorption spectroscopy of EXAFS spectra at the Mn K edge revealed further structural changes before the CV test. Because manganese oxide is amorphous after annealing at 250 °C, but is mainly crystalline Mn_2O_3 above 300 °C, the peaks shifted slightly to higher photon energy with temperature increases from 250 to 350 °C. (b) EXAFS spectra at Mn L_{III}-edge peaks. (c) Radial distribution functions (RDF) spectra. (d) EXAFS spectra from 700 to 735 eV at Fe L-edge peaks. The results showed that the first main peak of Mn–O atomic bonding was located at a 1.5 Å radius, and the second main peak of Mn–Mn atomic bonding was located at a

Table 2
Summary of comparison of specific capacitance (F/g) at varied composition of manganese oxide and annealing temperature.

Temp.	250 °C	300 °C	350 °C	400 °C
Un-added	40.7	101.2	71.6	57.8
0.5 Fe_3O_4 mol% adding	78.7	174.1	195.7	147.4
1.0 Fe_3O_4 mol% adding	69.6	210.8	232.3	165.7
2.0 Fe_3O_4 mol% adding	75.3	191.3	204.7	156.9
2.5 Fe_3O_4 mol% adding	72.4	167.1	191.2	113.6
5.0 Fe_3O_4 mol% adding	42.4	118.1	173.7	100.6
7.5 Fe_3O_4 mol% adding	24.0	99.2	136.8	84.2

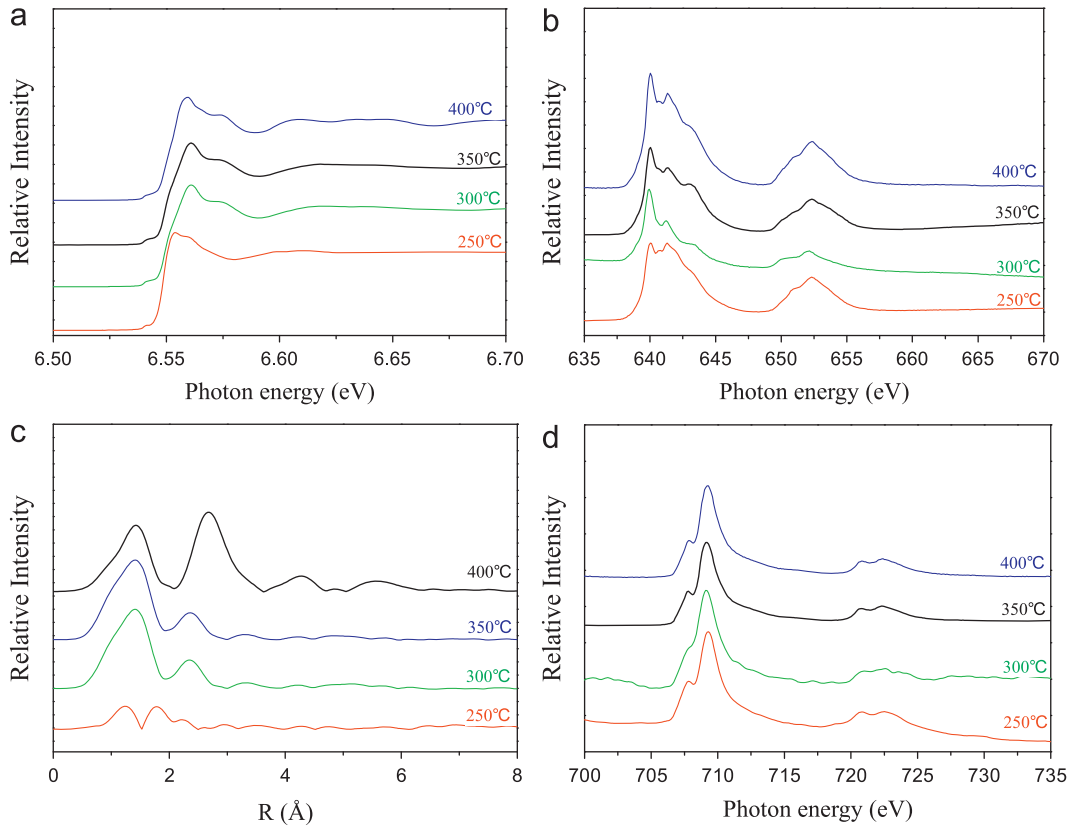

Fig. 9. Spectra of manganese oxide film with 1.0 mol% Fe addition after annealing at 250, 300, 350, and 400 °C: (a) synchrotron X-ray absorption spectroscopy of EXAFS spectra at the Mn K edge, (b) EXAFS spectra at Mn L_{III}-edge peaks, (c) radial distribution functions (RDF) spectra, and (d) EXAFS spectra from 700 to 735 eV at Fe L-edge peaks.

2.5 Å radius. The intensity of Mn–Mn peaks increased as annealing temperature increased. Thus, the crystallization of manganese oxide increased as annealing temperature increased and Fe L_{III} and L_{II} edge peaks were present at 708 and 721 eV respectively.

4. Conclusions

A pseudo-capacitive film of manganese iron oxide has been prepared by the sol–gel method. The manganese oxide film has a specific capacitance of 101.2 F/g after annealing at 300 °C. The specific capacitance of manganese oxide was improved with iron acetate addition and heat-treatment. The manganese/iron oxide films with 1.0 mol% Fe addition after annealing at 350 °C exhibited the best specific capacitance, 232.3 F/g, among the electrodes investigated in the present study. According to SEM observation and XRD detection, when 1.0 mol% Fe was added to manganese oxide film and the film was annealed at 350 °C, Mn $(OH)_x$ decomposed to Mn_3O_4 and Mn_2O_3 phases and formed many small pores on the film. Such small pores can increase the contact area between electrode and electrolyte and increase the specific capacitance.

Acknowledgments

The authors would like to thank the National Science Council of Taiwan and National United University for financially supporting this work. The authors also thank the entire staff at NSRRC (Hsinchu, Taiwan, ROC.) for their expert assistance.

References

[1] D.P. Dubal, C.D. Lokhande, Significant improvement in the electrochemical performances of nano-nest like amorphous MnO_2 electrodes due to Fe doping, Ceramics International 39 (2013) 415–423.
[2] B.E. Conway, Transition from supercapacitor to battery behavior in electrochemical energy storage, Journal of the Electrochemical Society 138 (1991) 1539–1548.
[3] S. Sarangapani, B.V. Tilak, C.P. Chen, Materials for electrochemical capacitors theoretical and experimental constraints, Journal of the Electrochemical Society 143 (1996) 3791–3799.
[4] R. Kötz, M. Carlen, Principles and applications of electrochemical capacitors, Electrochimica Acta 45 (2000) 2483–2498.
[5] W. Sugimoto, K. Yokoshima, K. Ohuchi, Fabrication of thin-film, flexible, and transparent electrodes composed of ruthenic acid nanosheets by electrophoretic deposition and application to electrochemical capacitors, Journal of the Electrochemical Society 153 (2006) A255–A260.
[6] J.P. Zheng, P.J. Cygan, T.R. Jow, Hydrous ruthenium oxide as an electrode material for electrochemical capacitors, Journal of the Electrochemical Society 142 (1995) 2699–2703.
[7] K.C. Liu, M.A. Anderson, Porous nickel oxide/nickel films for electrochemical capacitors, Journal of the Electrochemical Society 143 (1996) 124–130.
[8] Y.S. Yoon, W.I. Cho, J.H. Lim, D.J. Choi, Solid-state thin-film supercapacitor with ruthenium oxide and solid electrolyte thin films, Journal of Power Sources 101 (2001) 126–129.

[9] Z.J. Shen, W.P. Chen, K. Zhu, Y. Zhuang, Y.M. Hu, Y. Wang, H.L.W. Chan, Hydrogen-induced degradation in $SrTiO_3$-based grain boundary barrier layer ceramic capacitors, Ceramics International 35 (2009) 953–956.

[10] F.M. Filho, A.Z. Simões, A. Ries, L. Perazolli, E. Longo, J.A. Varela, Nonlinear electrical behaviour of the Cr_2O_3, ZnO, CoO and Ta_2O_5-doped SnO_2 varistors, Ceramics International 32 (2006) 283–289.

[11] I.H. Kima, K.B. Kima, Electrochemical characterization of hydrous ruthenium oxide thin-film electrodes for electrochemical capacitor applications, Journal of the Electrochemical Society 153 (2006) A383–A389.

[12] D. Bélanger, T. Brousse, J.W. Long, Manganese oxides: battery materials make the leap to electrochemical capacitors, Interface 17 (2008) 49–52.

[13] M. Toupin, T. Brousse, D. Bélanger, Charge storage mechanism of MnO_2 electrode used in aqueous electrochemical capacitor, Chemistry of Materials 16 (2004) 3184–3190.

[14] S.C. Pang, M.A. Anderson, T.W. Chapman, Novel electrode materials for thin-film ultracapacitors: comparison of electrochemical properties of sol–gel-derived and electrodeposited manganese dioxide, Journal of the Electrochemical Society 147 (2000) 444–450.

[15] S.R. Sivakkumar, J.M. Ko, D.Y. Kim, B.C. Kim, G.G. Wallace, Performance evaluation of CNT/polypyrrole/MnO_2 composite electrodes for electrochemical capacitors, Electrochimica Acta 52 (2007) 7377–7385.